Electronic spin and valence states of Fe in $CaIrO_3$-type silicate post-perovskite in the Earth's lowermost mantle

Z. Mao,[1] J. F. Lin,[1] C. Jacobs,[1] H. C. Watson,[2] Y. Xiao,[3] P. Chow,[3] E. E. Alp,[4] and V. B. Prakapenka[5]

Received 6 August 2010; revised 22 September 2010; accepted 30 September 2010; published 19 November 2010.

[1] The electronic spin and valence states of Fe in post-perovskite ($(Mg_{0.75}Fe_{0.25})SiO_3$) have been investigated by synchrotron X-ray diffraction, Mössbauer and X-ray emission spectroscopy at 142 GPa and 300 K. Rietveld refinement of the X-ray diffraction patterns revealed that our sample was dominated by $CaIrO_3$-type post-perovskite. Combined Mössbauer and X-ray emission results show that Fe in post-perovskite is predominantly Fe^{2+} (70%) in the intermediate-spin state with extremely high quadrupole splitting of 3.77(25) mm/s. The remaining 30% Fe can be assigned to two sites. Compared with recent studies, our results indicate that the intermediate-spin Fe^{2+} is stabilized in $CaIrO_3$-type post-perovskite over a wide range of Fe content, whereas the low-spin Fe^{3+} is more dominant in the 2 × 1 kinked post-perovskite structure. The characterization of these structural and compositional effects on the spin and valence states of Fe in post-perovskite can help in understanding the geochemical and geophysical behavior of the core-mantle region. **Citation:** Mao, Z., J. F. Lin, C. Jacobs, H. C. Watson, Y. Xiao, P. Chow, E. E. Alp, and V. B. Prakapenka (2010), Electronic spin and valence states of Fe in $CaIrO_3$-type silicate post-perovskite in the Earth's lowermost mantle, *Geophys. Res. Lett.*, *37*, L22304, doi:10.1029/2010GL045021.

1. Introduction

[2] $(Mg,Fe)SiO_3$ post-perovskite (PPv) is expected to be the most abundant phase in the Earth's D" region [*Murakami et al.*, 2004; *Oganov and Ono* 2004; *Tsuchiya et al.*, 2004]. The PPv phase is found to be stable in the $CaIrO_3$-type structure (*Cmcm*), but a number of kinked PPv structures, formed by sliding the {010} planes of the perovskite (Pv) structure with variation in the stacking sequence of SiO_6 octahedral layers, have also been reported [*Oganov et al.*, 2005; *Tschauner et al.*, 2008]. The occurrence of the $CaIrO_3$-type PPv and the related kinked phases has been used to explain seismological observations and geodynamic modeling of the lowermost mantle region [e.g., *Oganov et al.*, 2005; *Hirose*, 2006].

[3] It has been recently reported that Fe in PPv undergoes spin-pairing transitions under lower mantle pressures [e.g., *Lin and Tsuchiya*, 2008]. The spin transitions of Fe and variations in the Fe valence states can cause changes in density, elastic properties, electrical conductivity and radiative thermal conductivity of the lower mantle minerals [e.g., *Lin and Tsuchiya*, 2008; *Ohta et al.*, 2008; *Goncharov et al.*, 2010]. Deciphering the electronic spin and valence states of Fe in PPv thus provides new insights into the observed geophysical and geodynamic properties in the lowermost mantle [*Lin and Tsuchiya*, 2008]. Despite recent experimental and theoretical efforts, the Fe spin state in PPv remains highly debated, likely due to its presence in two valence states occupying different distorted crystallographic sites. For Fe^{2+} in particular, theoretical calculations suggested that it is in the high-spin (HS) state at all mantle pressures [*Stackhouse et al.*, 2006; *Zhang and Oganov*, 2006], whereas the only experimental study about Fe^{2+} showed that Fe^{2+} is in the intermediate-spin (IS) state in PPv with 40 mol.% Fe [*Lin et al.*, 2008]. We note that this relatively high iron content is above the theoretical percolation threshold where the Fe content is predicted to affect the electronic states in Pv, an analog to PPv [*Bengtson et al.*, 2008]. Furthermore, the occurrence of the kinked 2 × 1 structure ($P2_1/m$) was observed to significantly lower the Fe^{2+} content, but increase the Fe^{3+} in PPv [*Jackson et al.*, 2009]. These studies thus raise the question of how different PPv structures and compositions can affect the Fe spin and valence states.

[4] Here we have conducted synchrotron X-ray diffraction (XRD), synchrotron Mössbauer spectroscopy (SMS) and X-ray emission spectroscopy (XES) measurements on PPv with 25 mol.% Fe at lowermost mantle conditions. The presence of such Fe-rich PPv may explain the observed ultra-low velocity zone in the D″ region [*Garnero and McNamara*, 2008]. High-resolution XRD was used to refine the crystal structures of the synthesized PPv. SMS provides information on the site occupancies and hyperfine parameters of Fe in PPv [*Dyar et al.*, 2006], whereas XES can be used to quantitatively derive the total 3*d* spin momentum of Fe [*Vankó et al.*, 2006]. These combined results enable us to provide much needed constraints on the electronic spin and valence states of Fe in PPv with 25 mol.% Fe in the $CaIrO_3$-type structure.

2. Experiments

[5] ^{57}Fe-enriched polycrystalline enstatite, $(Mg_{0.75},Fe_{0.25})SiO_3$, was used as the starting material (auxiliary material).[1]

[1]Department of Geological Sciences, Jackson School of Geosciences, University of Texas at Austin, Austin, Texas, USA.
[2]Department of Geology and Environmental Geosciences, Northern Illinois University, Dekalb, Illinois, USA.
[3]HPCAT, Carnegie Institution of Washington, Advanced Photon Source, Argonne National Laboratory, Argonne, Illinois, USA.
[4]Advanced Photon Source, Argonne National Laboratory, Argonne, Illinois, USA.
[5]Center for Advanced Radiation Sources, University of Chicago, Chicago, Illinois, USA.

0094-8276/10/2010GL045021

[1]Auxiliary materials are available in the HTML. doi:10.1029/2010GL045021.

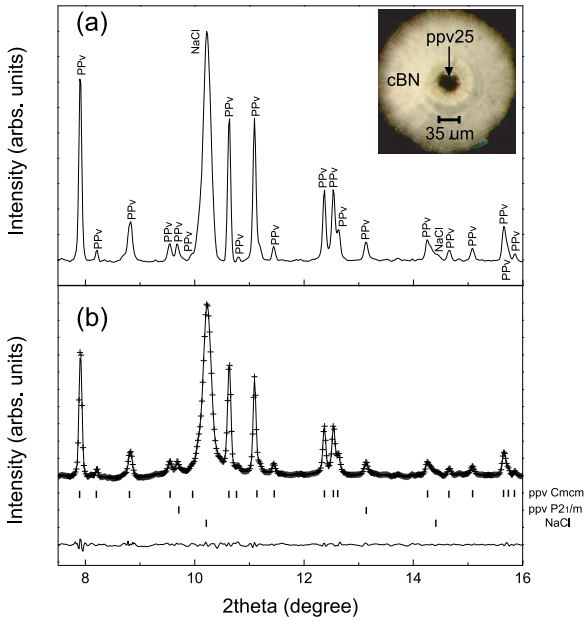

Figure 1. Angle-dispersive X-ray diffraction patterns of PPv. (a) PPv at 142 GPa and 300 K with lattice parameters a = 2.439(1) Å, b = 8.038(3) Å, and c = 6.077(2) Å. (b) Rietveld refinement of PPv with NaCl. Full-profile Rietveld refinement showed that approximately 96% of the synthesized sample was in the $CaIrO_3$-type PPv (*Cmcm*) phase, and the remaining PPv had a kinked 2 × 1 $P2_1/m$ structure. The line below the ticks represents the intensity difference between the collected X-ray data and refined results. Backgrounds of the spectra have been removed for clarity. Incident X-ray wavelength λ = 0.3344 Å.

The polycrystalline enstatite was compressed into disks of ~10 μm in thickness and 35 μm in diameter. The sample disk, sandwiched between two dried NaCl layers of 5 μm thick, was loaded in a diamond anvil cell having a preindented Be gasket with cBN gasket inserts and beveled diamonds (100 μm inner culet and 300 μm outer culet). The sample assemblage was compressed to ~142 GPa and laser heated at 2000 to 2500 K for eight hours to fully convert enstatite to PPv at 13-ID-D of the GSECARS, Advanced Photon Source (APS), Argonne National Laboratory (ANL). The sample was later used for XRD, XES and SMS experiments.

[6] XES measurements were conducted at HPCAT of the APS, ANL with an incident X-ray energy of 11.3 keV and an energy bandwidth of approximately 1 eV. Collection time for each XES spectrum was about 40 minutes, and 35 spectra were added together. A reference low-spin (LS) spectrum was collected from ferropericlase (fp25, $(Mg_{0.75}Fe_{0.25})O$) at 90 GPa [*Lin et al.*, 2010], whereas HS reference spectra were collected from perovskite (Pv10,$(Mg_{0.9}Fe_{0.1})SiO_3$), fp25 and enstatite ($(Mg_{0.75}Fe_{0.25})SiO_3$).

[7] High-pressure SMS experiments for enstatite and PPv were conducted at HPCAT of the APS, ANL with an energy resolution of approximately 2 meV. We took SMS spectra for samples with or without a stainless steel foil (≈10 μm thick with natural ^{57}Fe abundance) which was used as a reference to determine the chemical shift (CS) of the Fe sites. Collection time was approximately one hour for enstatite, and four to five hours for PPv.

3. Results

[8] The synthesis of PPv was confirmed by XRD (Figure 1). Rietveld full-profile refinement using GSAS/EXPGUI package [*Toby*, 2001] revealed that the sample was 96% dominated by the $CaIrO_3$-type PPv (*Cmcm*), except two relatively weak peaks at 1.9809 Å and 1.4621 Å (Table S1). These two peaks account for less than 4% in XRD intensity of the sample and can be assigned to the 2 × 1 type PPv ($P2_1/m$), a kinked structure of PPv formed by the variation in stacking sequence of octahedral layers (Figure 1) [*Oganov et al.*, 2005; *Tschauner et al.*, 2008].

[9] The XES spectra from three HS references, Pv10, fp25 and enstatite show negligible differences (less than 3% of the complete measured energy range) (Figure 2). We note that these samples contain various amount of HS Fe^{2+} and/or Fe^{3+} in different crystallographic sites. Based on both traditional and synchrotron Mössbauer analyses, the Pv10 sample contains approximately 75% HS Fe^{2+} in the A site and 25% HS Fe^{3+} which may occupy both dodecahedral and octahedral sites [*McCammon*, 1997; *Lin and Tsuchiya*, 2008]. The fp25 sample mainly consists of HS Fe^{2+} in octahedral sites. The enstatite sample contains 25 mol.% Fe^{2+} in both M1 and M2 sites. Comparison of these XES spectra shows that HS reference spectra are independent of the Fe site occupancy, valence states and crystallographic sites, validating the use of these spectra as the HS references. Here we have used fp25 at ambient conditions and 90 GPa as the HS and LS references, respectively.

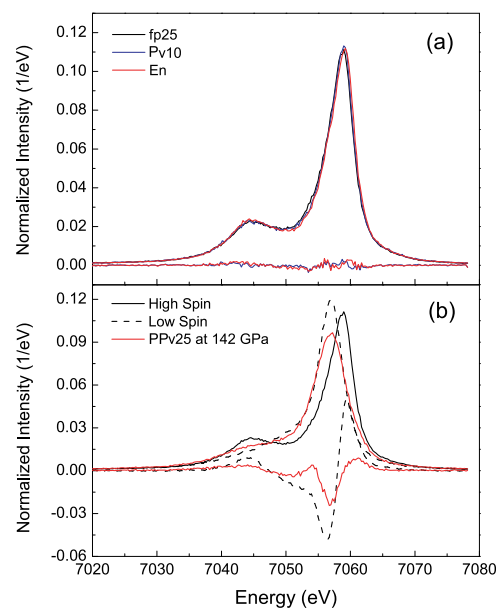

Figure 2. Normalized X-ray emission spectra of iron. (a) HS reference spectra: Pv10, fp25, and enstatite (En). The differences between Pv10 and fp25, En and fp25 are shown below the spectra. (b) PPv at 142 GPa and 300 K compared with HS (fp25) and LS references (fp25). The difference between the sample (or HS reference) and LS reference is shown below the X-ray emission spectra, and is within 3% of the measured spectra in both panels.

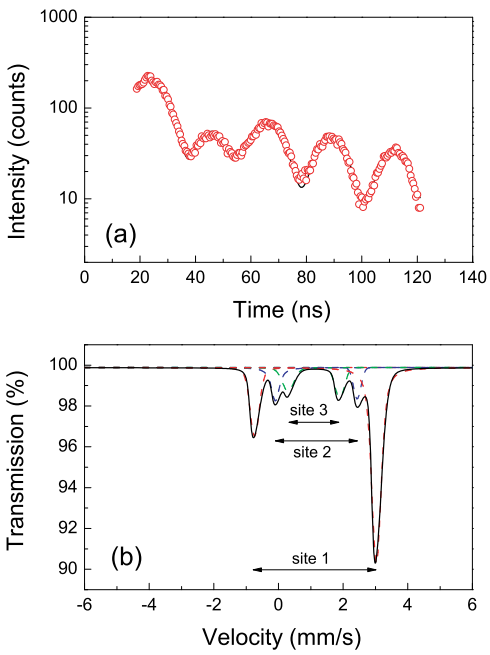

Figure 3. Mössbauer spectra of PPv at 142 GPa and 300 K. (a) Measured SMS spectrum (red circles) compared with the evaluated results (black lines). (b) Modeled energy spectrum from the evaluation of the SMS data in (a) with site 1 in red, site 2 blue and site 3 green.

[10] Compared to the HS reference, the XES spectrum of PPv shows a reduction in the intensity of the satellite emission peak (Kβ') and an energy shift of the Kβ main peak (Figure 2). We further evaluated the collected XES spectra using the Integrated Absolute Difference analysis (IAD) in which the absolute difference between the sample and LS reference is normalized and integrated [*Vankó et al.*, 2006]. Comparing this integral to that from the HS and LS references, we derived the total spin momentum, $S = 0.7(2)$.

[11] The SMS spectra were analyzed using the CONUSS program (Figures 3, S1, and S2 and Table S2) [*Sturhahn*, 2000]. Evaluation of the SMS spectra of PPv at 142 GPa and 300 K shows three distinct Fe sites with the most abundant site (site 1) dominated by extremely high quadrupole splitting (QS) and relatively high chemical shift (CS). Interpretation and assignment of the electronic states of the Fe sites are addressed in the discussion below.

4. Discussion and Geophysical Implications

[12] Fe exists as both Fe^{2+} and Fe^{3+} in PPv at lowermost-mantle conditions [*Sinmyo et al.*, 2006, 2008]. As shown from the SMS analyses of PPv (Table S2), site 1 with 70% abundance and QS = 3.77(25) mm/s can be assigned to be Fe^{2+} in the A site [*McCammon*, 1997; *Bengtson et al.*, 2009; *Jackson et al.*, 2009; *Catalli et al.*, 2010]. Since our XES analyses show S = 0.7(2), the most plausible explanation for the site 1 is the occurrence of the IS Fe^{2+} in the A site. This conclusion is consistent with that for PPv with 40 mol.% Fe [*Lin et al.*, 2008], but we emphasize that no Rietveld refinement was provided by *Lin et al.* [2008]. The remaining 30% of Fe occupies two distinct Fe sites. The site 2 with 17% occupancy and QS = 2.53(25) mm/s is assigned to be Fe^{3+} in the LS state, whereas the site 3 could be either LS Fe^{3+} or HS Fe^{3+}. Our assignment of the Fe^{3+} sites is primarily based upon the derived S number from XES and hyperfine parameters [*Xu et al.*, 2001; *Bengtson et al.*, 2009; *Catalli et al.*, 2010]. The amount of Fe^{3+} assigned to these two sites is consistent with literature values for Al-free PPv, in which 10–30% Fe^{3+} exists in quenched PPv [*Sinmyo et al.*, 2008]. Based on these discussion, we conclude that Fe in the $CaIrO_3$-type PPv phase is predominantly Fe^{2+} in the IS state in the lowermost mantle with a certain amount (10–30%) of Fe^{3+}. In light of our observations, the IS Fe^{2+} and LS Fe^{3+} in PPv would be the potential cause for the observed increase in the thermal and electrical conductivities in PPv [*Ohta et al.*, 2008; *Goncharov et al.*, 2010], and thus can greatly affect the dymanics of the lowermost mantle.

[13] Recent theoretical simulations indicate that Fe^{2+} in Pv is stable in the HS state but unstable in the IS state at all mantle pressures [*Bengtson et al.*, 2009; *Hsu et al.*, 2010]. Since PPv is the high-pressure polymorph of Pv, the QS of Fe^{2+} in PPv could be similar or related to that of Fe^{2+} in Pv. The calculated QS of Fe^{2+} in Pv is 3.3–3.6 mm/s at lower mantle pressures, consistent with our QS for Fe^{2+} in PPv. However, the occurrence of the Fe^{2+} site with extremely high QS is explained as a result of atomic-site change in the HS state [*Bengtson et al.*, 2009; *Hsu et al.*, 2010]. *McCammon et al.* [2008] have noted that high-degree lattice distortions exist in Pv and may help stabilize the IS Fe^{2+} through strong Jahn-Teller distortions (Table S1), and high temperature is generally expected to stabilize the IS spin state from 30 GPa [*McCammon et al.*, 2008]. Based on our Rietveld refinement results, our PPv sample also exhibits an increase in the octahedral tilting angles and a shortening of the bond length which could stabilize the IS Fe^{2+} by Jahn-Teller distortions (Table S1). Since much of our interpretation of the IS Fe^{2+} is based on the XES analyses, incorporation of the lattice distortions in future theoretical calculations as well as theoretical understanding of the XES spectra involving multiple electronic transitions are all needed to resolve the discrepancy between current experimental and theoretical results.

[14] Iron content in mantle minerals is known to affect the stability of Fe spin states [*Bengtson et al.*, 2008]. Since the IS Fe^{2+} in PPv is found stable with 25 mol% and 40 mol.% Fe, it is conceivable that the IS Fe^{2+} is stable over a wide range of Fe content in PPv relevant to the D" region, where Fe-enrichment may be expected. In addition, increasing Fe content in PPv does not affect the hyperfine fields of Fe^{2+} in the dodecahedral sites, whereas the QS of Fe^{3+} appears to increase with increasing Fe content (Figure S3) [*Lin et al.*, 2008; *Catalli et al.*, 2010].

[15] We note that our Mössbauer spectrum of PPv with 25 mol.% Fe is significantly different from that in PPv with 10 mol.% Fe by *Jackson et al.* [2009]. All of the Fe^{2+} is reported to disproportionate into Fe^{3+} and metallic Fe in PPv at 110 to 120 GPa by *Jackson et al.* [2009], whereas most of the Fe remains as Fe^{2+} in our study, consistent with *Lin et al.* [2008]. Although the structure refinement was not reported by *Lin et al.* [2008], re-examination of the X-ray diffraction pattern indicates PPv is mostly in the $CaIrO_3$-type structure [*Lin et al.*, 2008]. The PPv sample used by *Jackson et al.* [2009] is composed of multiple phases, including 60% $CaIrO_3$-type PPv, 30% 2 × 1 PPv, and 10% Pv. PPv in the kinked phases is predicted to be formed through a series of stacking-fault intermediate

between Pv and PPv by sliding the {010} planes of Pv. The corresponding plane slips in Pv might introduce more crystallographic defects favorable for Fe^{2+} to form Fe^{3+} and metallic Fe. On the other hand, it has been showed that PPv can contain certain amount of Fe^{3+} through self-oxidation reaction from Fe^{2+} [*Sinmyo et al.*, 2008]. Thus, the presence of the kinked PPv phase with Pv may influence the valence and spin states of Fe in PPv.

[16] In conclusion, our study here showed that $CaIrO_3$-type PPv predominantly contains the IS Fe^{2+} at lowermost mantle pressures, together with 30% Fe^{3+}. The Fe^{2+} is characterized by extremely high QS of 3.77(25) mm/s, and is assigned to be in the IS state in the $CaIrO_3$-type PPv using XRD, SMS and XES results. Together with the previous report of PPv with 40 mol.% Fe, we find that Fe^{2+} is stable in the IS state over a range of compositions relevant to the D" region. The site occupancy and the hyperfine parameters of Fe^{2+} are not significantly affected by the Fe content, but the addition of Fe increases the QS and decreases the CS of the minor Fe^{3+} sites. Although our observed extremely high QS and relatively high CS of Fe^{2+} in the A site are consistent with recent theoretical predictions, the most plausible interpretation for all of our experimental results is that Fe^{2+} is stable in the IS state in the $CaIrO_3$-type PPv at lowermost mantle pressures, whereas Fe in PPv with the kinked structures is predominant Fe^{3+} in the LS state.

[17] **Acknowledgments.** We acknowledge I. Kantor for experimental assistance and G. Vankó for discussion on the data analysis. Z. Mao and J. F. Lin acknowledge support from the US National Science Foundation (EAR-0838221), Energy Frontier Research in Extreme Environments (EFree), and the Carnegie/DOE Alliance Center (CDAC). C. Jacobs acknowledges NSF REU program and Thomas and Ray Burke Student Job Program of the Jackson School of Geosciences for financial support. This work was performed at HPCAT and GSECARS, APS, ANL supported through funding from DOE-NNSA, DOE-BES, NSF(EAR-0622171) and Department of Energy (DE-FG02-94ER14466).

References

Bengtson, A., K. Persson, and D. Morgan (2008), Ab initio study of the composition dependence of the pressure induced spin crossover in perovskite (Mg_{1-x},Fe_x)SiO_3, *Earth Planet. Sci. Lett.*, *265*, 535–545.

Bengtson, A., J. Li, and D. Morgan (2009), Mössbauer modeling to interpret the spin state of iron in (Mg,Fe)SiO_3 perovskite, *Geophys. Res. Lett.*, *36*, L15301, doi:10.1029/2009GL038340.

Catalli, K., S. H. Shim, V. B. Prakapenka, J. Zhao, and W. Sturhahn (2010), X-ray diffraction and Mössbauer spectroscopy of Fe^{3+}-bearing Mg-silicate post-perovskite at 128–138 GPa, *Am. Mineral.*, *95*, 418–421.

Dyar, M. D., D. G. Agresti, M. W. Schaefer, C. A. Grant, and E. C. Sklute (2006), Mössbauer spectroscopy of Earth and planetary materials, *Annu. Rev. Earth Planet. Sci.*, *34*, 83–125.

Garnero, E. J., and A. K. McNamara (2008), Structure and dynamics of Earth's lower mantle, *Science*, *320*, 626–628.

Goncharov, A. E., V. V. Struzhkin, J. A. Montova, S. Kharlamova, R. Kundargi, J. Siebert, J. Badro, D. Antonangeli, F. J. Ryerson, and W. Mao (2010), Effect of composition, structure, and spin state on the thermal conductivity of the Earth's lower mantle, *Phys. Earth Planet. Inter.*, *180*, 148–153.

Hirose, K. (2006), Postperovskite phase transition and its geophysical implications, *Rev. Geophys.*, *44*, RG3001, doi:10.1029/2005RG000186.

Hsu, H., K. Umemoto, P. Blaha, and R. M. Wentzcovitch (2010), Spin states and hyperfine interactions of iron in (Mg,Fe)SiO_3 perovskite under pressure, *Earth Planet. Sci. Lett.*, *294*, 19–26.

Jackson, J. M., W. Sturhahn, O. Tschauner, M. Lerche, and Y. Fei (2009), Behavior of iron in (Mg,Fe)SiO_3 post-perovskite assemblages at Mbar pressures, *Geophys. Res. Lett.*, *36*, L10301, doi:10.1029/2009GL037815.

Lin, J. F., and T. Tsuchiya (2008), Spin transition of iron in the Earth's lower mantle, *Phys. Earth Planet. Inter.*, *170*, 248–259.

Lin, J. F., et al. (2008), Intermediate-spin ferrous iron in lowermost mantle post-perovskite and perovskite, *Nat. Geosci*, *1*, 688–691.

Lin, J. F., Z. Mao, I. Jarrige, Y. Xiao, P. Chow, T. Okuchi, N. Hiraoka, and S. D. Jacobsen (2010), Resonant X-ray emission study of the lower-mantle ferropericlase at high pressures, *Am. Mineral.*, *95*, 1125–1131.

McCammon, C. (1997), Perovskite as a possible sink for ferric iron in the lower mantle, *Nature*, *387*, 694–696.

McCammon, C., I. Kantor, O. Narygina, J. Rouquette, U. Ponkratz, I. Sergueev, M. Mezouar, V. Prakapenka, and L. Dubrovinsky (2008), Stable intermediate-spin ferrous iron in lower-mantle perovskite, *Nat. Geosci.*, *1*, 684–687.

Murakami, M., K. Hirose, K. Kawamura, N. Sata, and Y. Ohishi (2004), Post-perovskite phase transition in $MgSiO_3$, *Science*, *304*, 855–858.

Oganov, A. R., and S. Ono (2004), Theoretical and experimental evidence for a post-perovskite phase of $MgSiO_3$ in Earth's D″ layer, *Nature*, *430*, 445–448.

Oganov, A. R., R. Martoňák, A. Laio, P. Raiteri, and M. Parrinello (2005), Anisotropy of Earth's D″ layer and stacking faults in the $MgSiO_3$ post-perovskite phase, *Nature*, *438*, 1142–1144.

Ohta, K., S. Onoda, K. Hirose, R. Shinmyo, K. Shimizu, N. Sata, Y. Ohishi, and A. Yasuhara (2008), The electrical conductivity of post-perovskite in Earth's D″ layer, *Science*, *320*, 89–91.

Sinmyo, R., K. Hirose, H. St. C. O'Neill, and E. Okunishi (2006), Ferric iron in Al-bearing post-perovskite, *Geophys. Res. Lett.*, *33*, L12S13, doi:10.1029/2006GL025858.

Sinmyo, R., H. Ozawa, K. Hirose, A. Yasuhara, N. Enro, N. Sata, and Y. Ohishi (2008), Ferric iron content in (Mg,Fe)SiO_3 perovskite and post-perovskite at deep lower mantle conditions, *Am. Mineral.*, *93*, 1899–1902.

Stackhouse, S., J. P. Brodholt, D. P. Dobson, and G. D. Price (2006), Electronic spin transitions and the seismic properties of ferrous iron-bearing $MgSiO_3$ post-perovskite, *Geophys. Res. Lett.*, *33*, L12S03, doi:10.1029/2005GL025589.

Sturhahn, W. (2000), CONUSS and PHOENIX: Evaluation of nuclear resonant scattering data, *Hyperfine Interact.*, *125*, 149–172.

Toby, B. H. (2001), EXPGUI, a graphical user interface for GSAS, *J. Appl. Crystallogr.*, *34*, 210–213.

Tschauner, O., B. Kiefer, H. Liu, S. Sinogeikin, M. Somayzulu, and S. N. Lou (2008), Possible structural polymorphism in Al-bearing magnesium-silicate post-perovskite, *Am. Mineral.*, *93*, 533–539.

Tsuchiya, T., J. Tsuchiya, K. Umemoto, and R. M. Wentzcovitch (2004), Phase transition in $MgSiO_3$ perovskite in the earth's lower mantle, *Earth Planet. Sci. Lett.*, *224*, 241–248.

Vankó, G., T. Neisius, G. Molnár, F. Renz, S. Kárpáti, A. Shukla, and F. M. F. de Groot (2006), Probing the 3D spin momentum with X-ray emission spectroscopy: The case of molecular-spin transitions, *J. Phys. Chem. B*, *110*, 11,647–11,653.

Xu, O. N., W. M, G. H. Rozenberg, M. P. Pasternak, and R. D. Taylor (2001), Pressure-induced breakdown of a correlated system: The progressive collapse of the Mott-Hubbard state in $RFeO_3$, *Phys. Rev. B*, *64*, 094411, doi:10.1103/PhysRevB.64.094411.

Zhang, F., and A. R. Oganov (2006), Valence state and spin transitions of iron in Earth's mantle silicates, *Earth Planet. Sci. Lett.*, *249*, 436–443.

E. E. Alp, Advanced Photon Source, Argonne National Laboratory, IL 60439, USA.

P. Chow and Y. Xiao, HPCAT, Carnegie Institution of Washington, Advanced Photon Source, Argonne National Laboratory, Argonne, IL 60439, USA.

C. Jacobs, J. F. Lin, and Z. Mao, Department of Geological Sciences, Jackson School of Geosciences, University of Texas at Austin, Austin, TX 78712, USA. (zhu.mao@jsg.utexas.edu)

V. B. Prakapenka, Center for Advanced Radiation Sources, University of Chicago, Chicago, IL 60637, USA.

H. C. Watson, Department of Geology and Environmental Geosciences, Northern Illinois University, Dekalb, IL 60115, USA.